Journal of
Materials Chemistry C

Materials for optical, magnetic and electronic devices

Accepted Manuscript

This article can be cited before page numbers have been issued, to do this please use: C. P. Muzzillo, C. L. Perkins, S. Grover and A. Zakutayev, *J. Mater. Chem. C*, 2026, DOI: 10.1039/D6TC00099A.

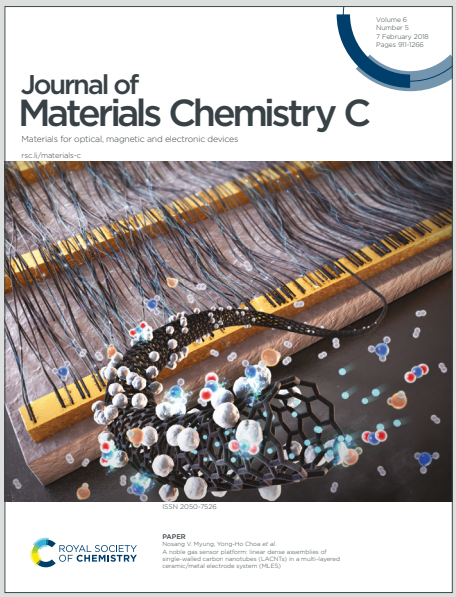

ROYAL SOCIETY OF CHEMISTRY

rsc.li/materials-c

View Article Online
DOI: 10.1039/D6TC00099A

Nitrogen p-type doping in polycrystalline zinc selenide telluride films

Christopher P. Muzzillo,[1*] Craig L. Perkins,[1] Sachit Grover,[2] and Andriy Zakutayev[1]

[1]Materials Science Center, National Laboratory of the Rockies, Golden, CO 80401

[2]California Technology Center, First Solar Inc., Santa Clara, CA 95050

*Corresponding author email: christopher.muzzillo@nrel.gov

Abstract

Nitrogen-doped zinc selenide telluride (N:$ZnSe_xTe_{1-x}$) is of interest because it is one of the widest-gap II-VI semiconductors that can still be doped p-type with reasonably high hole concentrations. We sputter deposit N:$ZnSe_xTe_{1-x}$ films, varying Se/(Se+Te), or x, from 0 to 0.7, N_2 flow rate from 0.25 to 0.75 sccm, and substrate temperature from 250 to 370 °C. Increasing x from 0 to 0.39 at the optimal temperature of 370 °C and N_2 flow rate of 0.5 sccm leads to 1.3 at. % nitrogen incorporation and wurtzite phase stabilization. Such doping and alloying increases hole concentration from 3×10^{18} cm^{-3} to 3×10^{19} cm^{-3}, although mobility drops from 0.4 to 0.02 cm^2 V^{-1} s^{-1}. Our sputtered N:$ZnSe_{0.38}Te_{0.62}$ has an absorption onset 0.1 eV greater than the ZnTe value of 1.87 eV. Increasing x from 0 to 0.51 enhances transmittance by moving absorption onset from 1.87 to 2.11 eV with diminished band gap bowing likely due to disorder, and increases the work function from 5.12 to 5.42 eV. This combination of tunable properties makes sputtered N:$ZnSe_xTe_{1-x}$ desirable for transparent p-type contacts in polycrystalline Cd(Se,Te) optoelectronic devices.

Introduction

Nitrogen-doped zinc selenide telluride (seleno-telluride; N:$ZnSe_xTe_{1-x}$) is interesting for optoelectronic applications because it is one of the widest-band gap II-VI semiconductors that can be doped p-type with reasonably high hole concentrations. Both ZnSe and ZnTe typically assume the zincblende crystal structure, although the wurtzite polymorph has been reported for ZnTe,[1] nanocrystalline ZnSe,[2] and $ZnSe_xTe_{1-x}$ alloys.[3] Its potential applications include hole selective contacts for Cd(Se,Te) solar cells[4, 5] and photoelectrochemical (PEC) carbon dioxide (CO_2) reduction cells.[6-10] It is also used in green and blue light-emitting diodes,[11-17] lasers,[18, 19] visible and ultraviolet photodetectors,[7, 10, 20] spintronic devices,[21, 22] and scintillators.[23, 24]

In particular for CdTe solar cells,[20, 25] which is the thin-film photovoltaic (PV) absorber with the greatest deployment worldwide,[26] N:ZnTe is primarily used as the p-type contact. The CdTe has a high electron affinity (4.3 to 4.5 eV[27, 28]), a high work function (up to 5.7 eV[27]) and defect chemistry that pins the Fermi level, which can lead to

View Article Online
DOI: 10.1039/D6TC00099A

electrical barriers at its interfaces.[26, 27] Resistance in the N:ZnTe (10^3 Ω/sq), resistance in the CdTe (10^4 Ω/sq), and recombination at their interface can also limit CdTe PV.[29] As the CdTe absorbers are alloyed with CdSe to tune the band gap and improve performance, the interface contact challenges can become even more difficult to address. Therefore, alloying ZnTe with ZnSe, and nitrogen doping the resulting zinc selenide telluride (N:$ZnSe_xTe_{1-x}$) would be attractive for Cd(Se,Te) devices, if it can improve on doping and band alignment relative to N:ZnTe.

$ZnSe_xTe_{1-x}$ single crystals and epitaxial films have been successfully doped with nitrogen,[19, 30-32] with hole concentrations demonstrated up to 10^{20} cm^{-3} at Se/(Se+Te) (or x) of 0.6.[31] Alloying ZnSe with Te has been reported to improve activation of nitrogen dopants.[19] Phosphorus[33] and arsenic[34] dopants have also been used in epitaxial layers. Polycrystalline $ZnSe_xTe_{1-x}$ films have been studied in several papers,[3-5, 21, 23, 35-44] but there are only three studies on p-type doping polycrystalline $ZnSe_xTe_{1-x}$.[3-5] Conductivities of 2 × 10^{-8} S/cm[4] and 10^{-3} S/cm[5] were reported in the initial publications. More recently the stabilization of the wurtzite polymorph was documented along with a 10^{19} cm^{-3} hole concentration in nitrogen doped $ZnSe_{0.5}Te_{0.5}$.[3]

Here we sputter deposit N:$ZnSe_xTe_{1-x}$ films and study their optoelectronic properties. We alter N_2 flow during sputtering and co-deposit from ZnTe and ZnSe targets to make a compositional gradient. We find hole concentration optima at N_2 flow of 0.5 sccm and Se/(Se+Te) (x) composition of 0.39. High temperature growth (370 °C) yields hole concentrations up to 3 × 10^{19} cm^{-3} at x of 0.39 and nitrogen concentration of 1.3% in the wurtzite structure, which is a tenfold improvement relative to x of 0. Increasing x from 0 to 0.51 monotonically increases work function from 5.12 to 5.42 eV and absorption onset energy from 1.87 to 2.11 eV, as the disorder in polycrystalline thin films likely reduces band gap bowing. These semiconductor properties make N:$ZnSe_xTe_{1-x}$ interesting for transparent p-type contact applications in Cd(Se,Te) and other optoelectronic devices.

Results and Discussion

We examine $ZnSe_{0.36}Te_{0.64}$ films sputtered with different N_2 flow rates by x-ray photoelectron spectroscopy (XPS) in Fig. 1a. The N 1s peak intensity shows that higher N_2 flow during sputtering leads to more N in the film. The N 1s binding energy of 396.15 eV is consistent with nitrogen present as N^{3-} with zinc coordination, the desired chemical state for a Group V acceptor in $ZnSe_xTe_{1-x}$.[45] The measured N concentration increases from 0.6 to 2.5 total atomic % as the flow rate increases from 0.25 to 0.75 sccm, as shown in Fig. 1b. XPS survey scans and Zn $2p_{3/2}$, Te 4d, Se 3d, N 1s, and O 1s high resolution core levels are in Fig. S1. For a constant 0.5 sccm N_2 flow rate, increasing x from 0 to 0.5 decreases N incorporation. XPS shows 10 to 34% greater x than x-ray fluorescence

View Article Online
DOI: 10.1039/D6TC00099A

(XRF) in Table S1 and Fig. S2, which compare XRF and XPS compositions. Se surface enrichment is unlikely, as there is little peak shift with grazing incidence XRD (GIXRD) incidence angle (Fig. S3). Therefore, our use of pure element XPS sensitivity factors may be incorrectly shifting x higher in Fig. S2.

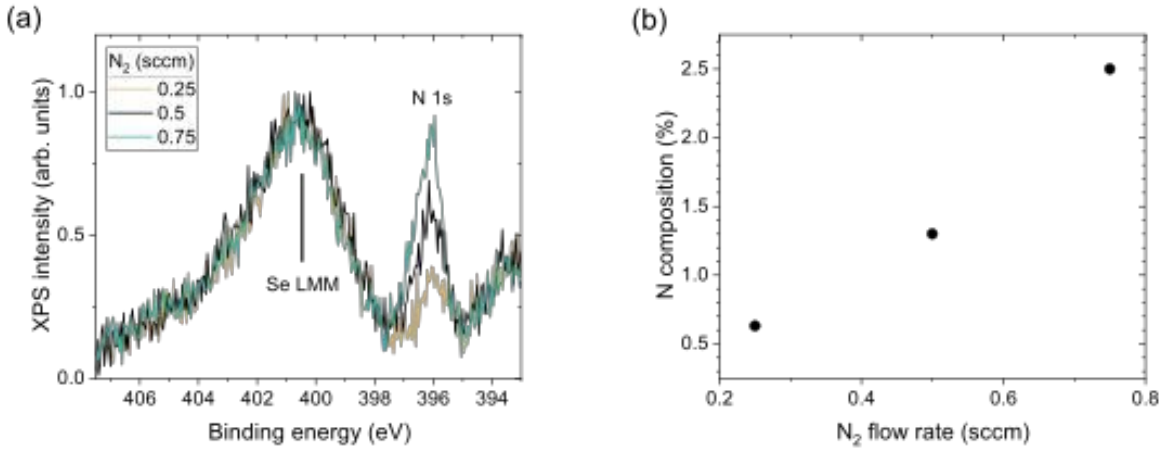

Fig. 1. Composition measurements: (a) XPS N 1s spectra and (b) N composition in total atomic % of $ZnSe_{0.36}Te_{0.64}$ films grown at 370 °C with varied N_2 flow, showing that N_2 flow during sputtering correlates with N in the film.

Hall effect shows that increasing growth temperature from 250 to 370 °C increases hole concentration. Increasing N_2 from 0.25 to 0.5 sccm slightly increases hole concentration, but increasing N_2 from 0.5 to 0.75 sccm apparently deactivates N (Fig. 2a). The hole concentration—mobility tradeoff is also best for N_2 flow of 0.5 sccm. Similar to N_2 flow, increasing x from 0 to 0.4 increases hole concentration, but p sharply drops at x > 0.4 (Fig. 2b). Increasing N_2 flow is also known to favor the wurtzite structure relative to sphalerite (zincblende),[3] but that should not influence p-type doping because we find no differences in doping or band edge between the different polytypes.

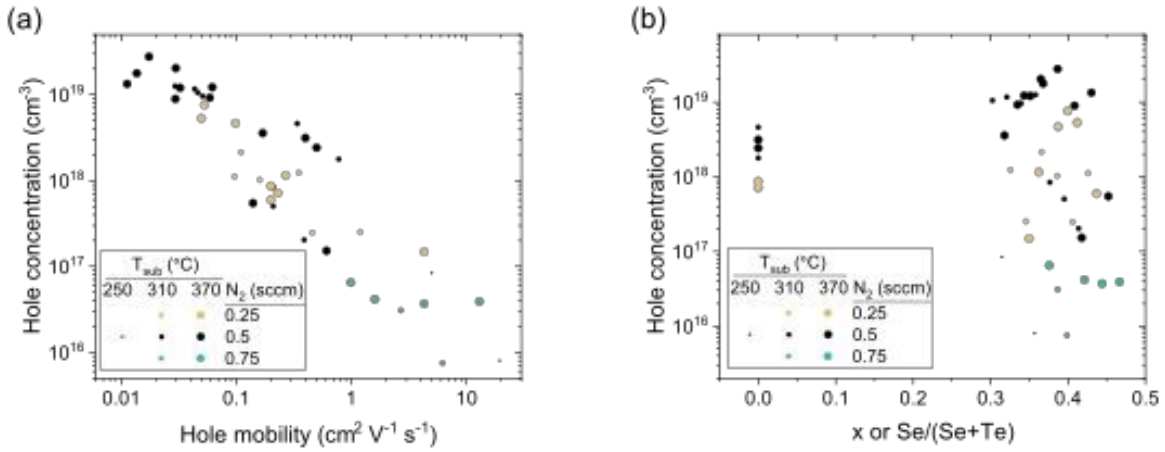

View Article Online
DOI: 10.1039/D6TC00099A

Fig. 2. Hole concentration versus hole mobility for all x compositions (a) and x or Se/(Se+Te) (b) for films with x from 0 to 0.49 grown at varied substrate temperature and N_2 flow.

At N_2 of 0.5 sccm, films with x of 0 and 0.34 have the sphalerite structure, but increasing x from 0.38 to 0.47 increases the wurtzite x-ray diffraction (XRD) peak intensities (Fig. S4). XRD in Fig. S4 further shows that at x of 0.47, increasing N_2 flow favors the wurtzite even more than at lower x. ZnSe (x of 1) has the sphalerite structure again (Fig. 3a), in agreement with density functional theory (DFT) predicting wurtzite stability only at moderate x and N compositions.[3] Fig. 3b depicts the wurtzite stabilization at moderate x composition and N_2 flow, while Fig. S5 has the sphalerite and wurtzite lattice parameter variation with x composition. Fig. S5 shows that our films have larger lattice parameters than the bulk ZnTe and ZnSe values, a possible indicator of tensile strain. Fig. S6 has magnified (111) XRD reflections near 25.3° 2θ for x of 0, showing that increasing N_2 flow from 0.25 to 0.5 sccm decreases full width at half maximum and lattice parameter. Thus, the optimal N_2 flow of 0.5 sccm may form more nitrogen-on-anion (N_{Te} and N_{Se}) acceptors, which add disorder and shrink the lattice (Fig. S6) while enhancing p-type doping (Fig. 2). The lattice parameter stops shifting around x of 0.67 in Fig. S5, which could relate to the Zn-Se bond lengths staying relatively constant as ZnSe is alloyed with Te.[22, 46-48]

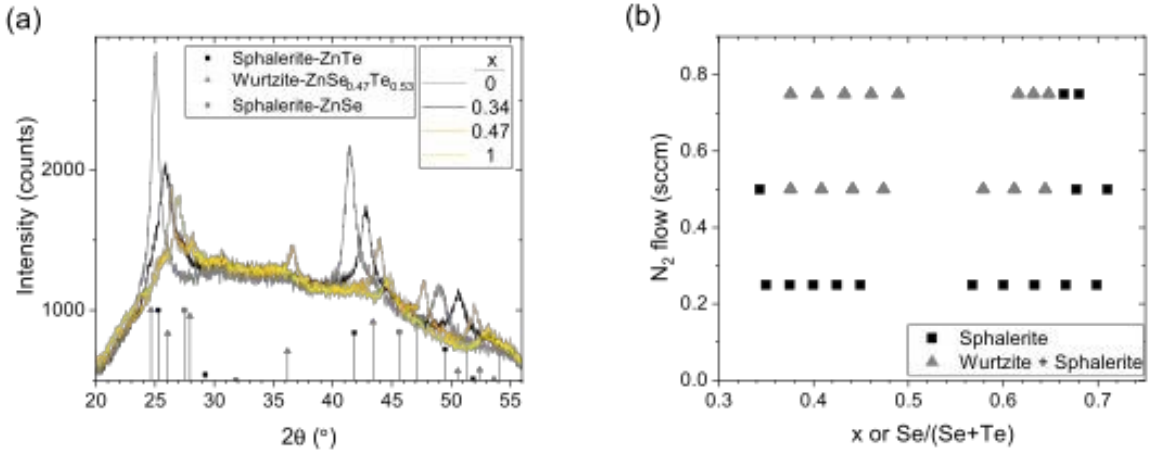

Fig. 3. Structural properties: (a) XRD of films with x varied from 0 to 1 and N_2 of 0.5 sccm grown at 370 °C, along with calculated sphalerite-ZnTe, wurtzite-$ZnSe_{0.47}Te_{0.53}$ and sphalerite-ZnSe peaks, and (b) a phase map of polytype XRD peaks, showing that sphalerite is stable at low and high x, and N_2 stabilizes wurtzite relative to sphalerite at moderate x.

View Article Online
DOI: 10.1039/D6TC00099A

We find that increasing x monotonically increases absorption onset energy (Fig. 4a), showing not much band gap bowing (Fig. 4b). This is surprising because former reports on single crystal,[49-53] epitaxial,[54-58] and DFT[59-63] $ZnSe_xTe_{1-x}$ find large band gap bowing, usually a decrease of 0.1 to 0.2 eV with a minimum near x of 0.3 to 0.35. On the other hand, evaporated and electrodeposited films have linearly increasing band gaps with x (that is, no band gap bowing).[21, 23, 37, 39, 41, 42, 44] From x of 0 to 0.34, the Tauc plot in Fig. S7 shows band gap widening by 0.12 eV instead of the 0.05 eV narrowing in Fig. 4. Thus, the Tauc plot has more band gap bowing and better quantitative agreement with reported single crystal $ZnSe_xTe_{1-x}$ band gaps, so disorder may diminish bowing in the absorption onset energy (Fig. 4), where we choose an absorption onset threshold of 10^4 cm^{-1} to minimize the effect of film smoothness-caused interference fringes. DFT finds a connection between disorder and band gap bowing,[55, 60-64] and some DFT studies have predicted far less band gap bowing in $ZnSe_xTe_{1-x}$.[18, 61, 63, 65-68] In Te-rich $ZnSe_xTe_{1-x}$ alloys the Zn-Te bonds are the same length as in ZnTe and in Se-rich $ZnSe_xTe_{1-x}$ the Zn-Se bonds are the same length as in ZnSe,[22, 46-48] which may relate to the link between order and band gap bowing. We also note that in the literature introducing N into ZnTe films *decreases* the apparent band gap,[69-72] so more work is needed to separate band gap bowing, disorder from sputtering and N incorporation, x shifts, and defect energies such as N_{Se} and N_{Te} acceptors.

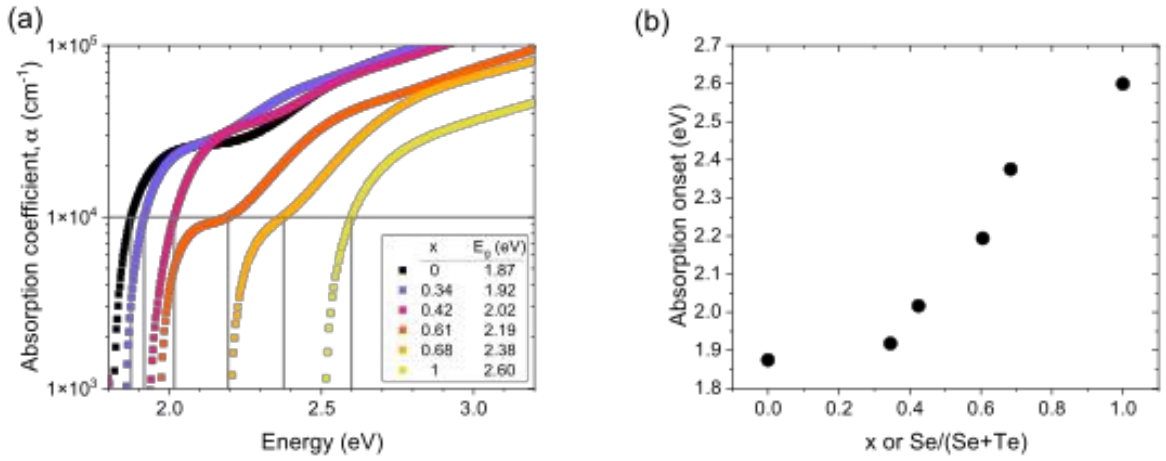

Fig. 4. Optical properties: (a) UV-visible spectroscopy log10 absorption coefficient plot for films with x of 0 to 1 and N_2 of 0.5 sccm grown at 370 °C. (b) The gray line at $1 \cdot 10^4$ cm^{-1} in (a) intercepts the data to show a monotonic absorption onset energy increase with x.

Kelvin probe measurements show a nearly linear increase in work function with x for N_2 of 0.25 sccm (Fig. 5a). Increasing N_2 flow appears to separate more highly doped material at low $x < 0.6$ from less doped material at $x > 0.6$, the latter of which greatly increases work function by lowering the valence band. Fig. S8 has XPS secondary electron cutoff (SECO) for different x composition and N_2 flow rates, showing similar work

View Article Online
DOI: 10.1039/D6TC00099A

function trends at greater magnitudes, relative to Kelvin probe (Fig. 5). Extrapolating E_F-E_V from ultraviolet photoelectron spectroscopy (UPS) on a logarithmic scale (Fig. S9) shows similar E_F-E_V as Hall effect data for the different N_2 flow rates (Table 1).

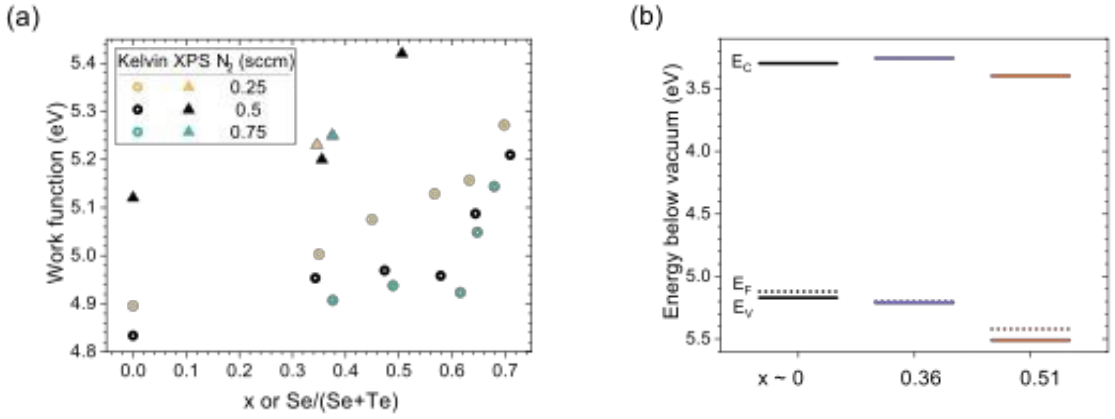

Fig. 5. (a) Kelvin probe (rings) and XPS-extracted work functions as a function of x for films grown at 370 °C and varied N_2 flow. (b) Energy band alignment for N:$ZnSe_xTe_{1-x}$ with varied x and N_2 of 0.5 sccm grown at 370 °C, incorporating XPS SECO work function, Hall E_F-E_V, and UV-visible spectroscopy absorption onset energy.

The complete picture of band positions for 0.5 sccm N_2 is shown in Fig. 5b. We use the XPS work functions because unlike Kelvin probe data, XPS data yield absolute functions. Perhaps for this reason, they are in better agreement with a former report.[28] As x is increased from 0 to 0.36, the band gap widens 0.08 eV, the Fermi energy decreases 0.08 eV, and the valence band decreases by 0.04 eV. As x is increased from 0.36 to 0.51, the band gap widens 0.16 eV, the Fermi energy drops another 0.22 eV, and the valence band drops another 0.3 eV. Thus, hole concentrations are optimal for x of 0.3 to 0.4 (Fig. 2), while lower valence band alignment is achieved at x of 0.5 to 0.7 (Fig. 5). Since alloying N:ZnTe with Se increases transmittance, increases hole concentration, and lowers the valence band (Table 1), we conclude that N:$ZnSe_xTe_{1-x}$ is an attractive alternative to N:ZnTe for p-type contacts in optoelectronics.

Table 1. Summary of key results. Hole concentration is p, hole mobility is μ_p, conductivity is σ, and work function is φ. An asterisk (*) means the E_F-E_V is estimated assuming resistivity is proportional to p. A double asterisk (**) means the band gap is interpolated from other x compositions.

XRF x or Se/(Se+Te)	0	0.35	0.36	0.38	0.51	0.68
N_2 (sccm)	0.5	0.25	0.5	0.75	0.5	0.5
p (cm^{-3})	3.1×10^{18}	1.5×10^{17}	1.2×10^{19}	6.5×10^{16}	5.5×10^{17}	-

View Article Online
DOI: 10.1039/D6TC00099A

μ_p (cm^2/V s)	0.40	4.3	0.062	0.99	0.14	-
σ (S/cm)	0.20	0.10	0.12	0.010	0.012	4×10^{-3}
Hall E_F-E_V (eV)	0.05	0.12	0.01	0.15	0.09	0.28*
UPS E_F-E_V (eV)	0.23	0.21	0.29	0.33	0.40	-
Kelvin φ (eV)	4.83	5.00	4.95	4.91	4.97	5.21
XPS φ (eV)	5.12	5.23	5.20	5.25	5.42	-
E_g (eV)	1.87	1.94**	1.95**	1.98**	2.11**	2.38

Conclusions

For sputter deposited polycrystalline N:$ZnSe_xTe_{1-x}$ at optimal temperature of 370 °C and N_2 flow of 0.5 sccm resulting in 1.3% N incorporation, increasing x from 0 to 0.39 improves hole concentration from 3×10^{18} cm^{-3} to 3×10^{19} cm^{-3}, although mobility drops from 0.4 to 0.02 cm^2 V^{-1} s^{-1}. Increasing x from 0 to 0.38 *increases* absorption onset energy by 0.1 eV because band gap bowing is diminished, likely due to disorder. Increasing x from 0 to 0.51 increases work function from 5.12 to 5.42 eV and increases transmittance by shifting the absorption onset energy from 1.87 to 2.11 eV. The increased work function, shifted absorption onset and higher hole concentration together make N:$ZnSe_xTe_{1-x}$ attractive for transparent p-type contact application in Cd(Se,Te) and other optoelectronic devices.

Methods

We clean 2 in x 2 in soda-lime glass (SLG) substrates with a thickness of 2.3 mm by ultrasonication in hot de-ionized (DI) water with Liquinox soap for 20 min. We then rinse thoroughly with DI water and blow with N_2 until completely dry. Starting at a base pressure of 10^{-7} Torr, we radio frequency (RF) co-sputter in 2.7 mTorr Ar (16 sccm) from ZnTe and ZnSe targets (99.99%; 2 in diameter; 0.125 in thick) at 20 W and 40 W, respectively. Depositing for 60 min leads to 300 – 500 nm thick films. The ZnTe and ZnSe targets are on opposite sides of the chamber, 37° off-normal to the substrate, and we co-deposit on stationary substrates to grow a compositional gradient across the substrates. We ramp substrate temperature to 370, 310, or 250 °C over the course of 50 min and pre-sputter for 10 min before opening the target shutters. We flow 0.25, 0.5 or 0.75 sccm N_2 through a gas distributor near the substrates and do not use an N_2 cracker.

We use XRF to measure film composition with a Rh anode at 50 kV for 60 s at 22 locations across each 2 in x 2 in sample, quantifying relative Se and Te content with Fischer XDV-SDD WinFTM software. We cut 5 mm x 5 mm squares and use silver paint contacts for Hall effect measurements at 1 T. We convert hole concentration to E_F-E_V

View Article Online
DOI: 10.1039/D6TC00099A

assuming a valence band density of states (N_V) of 1.8 × 10^{19} cm^{-3}.[73] We perform symmetric θ-2θ XRD with a Bruker D8 using monochromated Cu Kα radiation with a 1 mm spot and a 2-dimensional detector, integrating over χ. We do not correct for the 2D detector pixels' angular coverage,[74] so the lower intensity at 2θ of 20° – 23° is related to the diffractometer. We perform GIXRD on a Rigaku Smartlab diffractometer with a 2 mm spot in parallel beam geometry. We simulate diffraction patterns of $ZnSe_xTe_{1-x}$ by interpolating the lattice parameters of the ZnTe sphalerite (a = 6.102 Å),[75] wurtzite (a = 4.31 Å; c = 7.09 Å),[76] ZnSe wurtzite (a = 4.003 Å; c = 6.54 Å),[77] and ZnSe sphalerite (a = 5.62 Å)[78] end-members (Vegard's law). We fit lattice parameters to experimental patterns by matching multiple simulated XRD peak positions. We perform UV-visible spectroscopy with a Cary 6000 spetrophotometer and a diffuse reflectance integrating sphere. We combine transmissivity (T), reflectivity (R) and thickness (t; from stylus profilometry) to construct Tauc plots, where absorption coefficient, $\alpha = \ln[(1-R)^2 / T] / t$.[79] We square the product of α, Planck's constant (h), and photon frequency (v) and use a least-squares fit on the linear region, extrapolating to α = 0 for band gap. We use a Kelvin probe to measure work function by calibrating to Au and Al.

For films used in XPS measurements, instead of SLG we use Tec-15 substrates (SLG/diffusion barrier/SnO_2:F). We make electrical contact to the SnO_2:F layer using a molybdenum mask. We perform XPS measurements at near-normal electron-take off angle using monochromatic Al Kα radiation in a customized Physical Electronics VersaProbe III. High energy resolution XPS spectra were quantified into "equivalent homogeneous compositions"[80] using literature sensitivity factors and Shirley backgrounds. We collect wide range "survey" spectra using 280 eV pass energy to assure sample cleanliness. We clean air-exposed films using a gas cluster ion source (15 kV Ar_{2000}^+) until no extrinsic impurities can be observed. We perform work function measurements using low power x-ray excitation with a -5 V bias, and a pass energy of 6.5 eV. Under these conditions and using XPS analyzer settings, with He I radiation (21.22 eV) the Fermi edge of clean gold is located at 1460.5 eV. We use x-rays rather than UPS in work function determinations to avoid a helium lamp induced artifact observed on some materials.[81] We obtain valence band edges from log10 plots of UPS data, a procedure that captures low density of states (DOS) edges that can evade detection by linearly scaled XPS or UPS spectra.[82, 83] We take core level spectra (pass energy 55 eV) with and without exposure to our polychromatic helium lamp to test for possible source-induced photovoltages during UPS: we observe none. We numerically subtract satellites in UPS spectra after measuring the relative intensities of the satellites from spectra of the Fermi edge feature of clean gold foil. We calibrate the binding energy scale of the XPS and UPS experiments using the Fermi edge feature of clean metal foils and the literature values of copper $2p_{3/2}$ (932.67 eV) and gold $4f_{7/2}$ (83.98 eV).[84] We work up data using a combination of Physical Electronics MultiPak v9.9.1.1 and Wavemetrics Igor Pro 9.

View Article Online
DOI: 10.1039/D6TC00099A

Conflicts of interest

There are no conflicts of interest to declare.

Acknowledgment

This work was authored by NLR for the U.S. Department of Energy (DOE), operated under contract No. DE-AC36-08GO28308. Funding for structural and optoelectronic characterization was provided by the Liquid Sunlight Alliance, which is supported by the U.S. Department of Energy, Office of Science, Office of Basic Energy Sciences, Fuels from Sunlight Hub, under award number DE-SC0021266. Support for the thin film growth was provided by First Solar Inc. under Agreement 10543 CRD13507. The authors gratefully acknowledge the help of Jocienne Nelson. The views expressed in the article do not necessarily represent the views of the DOE or the U.S. Government.

References

1. K. V. Shalimova, I. Spinulescu-Carnaru and N. V. Pirogova, *Soviet Physics Journal*, 1966, **9**, 9-10.
2. D. D. Hile, H. C. Swart, S. V. Motloung, T. E. Motaung and L. F. Koao, *Physica B: Condensed Matter*, 2019, **575**, 411706.
3. T. H. Culman, R. Woods-Robinson, J. S. Mangum, R. W. Smaha, C. L. Rom, A. Zakutayev and S. R. Bauers, *Journal of Materials Chemistry C*, 2022, **10**, 15806-15815.
4. S. Vakkalanka, C. S. Ferekides and D. L. Morel, *Thin Solid Films*, 2007, **515**, 6132-6135.
5. S. Vakkalanka, C. S. Ferekides and D. L. Morel, *Proceedings of the 33rd IEEE Photovoltaic Specialists Conference*, 2008, DOI: 10.1109/PVSC.2008.4922534, 1-4.
6. E. Elsayed and A. Y. Shenouda, *Egyptian Journal of Chemistry*, 2022, **65**, 623-633.
7. S. Hussain, L. Guo and T. He, *The Journal of Physical Chemistry C*, 2021, **125**, 16235-16245.
8. C. P. Muzzillo, Y. Lai, J. A. Haber and A. Zakutayev, *ACS Applied Energy Materials*, 2025, **8**, 983-990.
9. A. K. Singh, J. H. Montoya, J. M. Gregoire and K. A. Persson, *Nature Communications*, 2019, **10**, 443.
10. S. Hussain, X. Yang, J. Yang and Q. Li, *Materials Today Sustainability*, 2024, **25**, 100686.
11. H. Asano, K. Arai, M. Kita and T. Omata, *Materials Research Express*, 2017, **4**, 106501.

View Article Online
DOI: 10.1039/D6TC00099A

12. H. Asano, S. Tsukuda, M. Kita, S. Fujimoto and T. Omata, *ACS Omega*, 2018, **3**, 6703-6709.
13. G. Jia, Y. Wang, L. Gong and J. Yao, *Digest Journal of Nanomaterials & Biostructures (DJNB)*, 2011, **6**.
14. T. Kim, K.-H. Kim, S. Kim, S.-M. Choi, H. Jang, H.-K. Seo, H. Lee, D.-Y. Chung and E. Jang, *Nature*, 2020, **586**, 385-389.
15. C. Li, K. Nishikawa, M. Ando, H. Enomoto and N. Murase, *Journal of Colloid and Interface Science*, 2008, **321**, 468-476.
16. K. G. Sonawane, C. Rajesh and S. Mahamuni, *Advanced Nanomaterials and Nanotechnology*, 2013, 261.
17. Q. Wu, F. Cao, W. Yu, S. Wang, W. Hou, Z. Lu, W. Cao, J. Zhang, X. Zhang, Y. Yang, G. Jia, J. Zhang and X. Yang, *Nature*, 2025, **639**, 633-638.
18. B. Freytag and U. Rössler, *Journal of Crystal Growth*, 1994, **138**, 499-503.
19. W. Lin, S. P. Guo, M. C. Tamargo, I. Kuskovsky, C. Tian and G. F. Neumark, *Applied Physics Letters*, 2000, **76**, 2205-2207.
20. A. E. Rakhshani, *Thin Solid Films*, 2013, **536**, 88-93.
21. V. S. Nagarethinam, M. G. S. B. Ahamed, K. Vijayakumar, L. Amalraj, A. R. Balu, A. Thayumanavan, K. R. Murali, C. Sanjeeviraja and M. Jayachandran, *Journal of Materials Science: Materials in Electronics*, 2011, **22**, 607-613.
22. P. F. Peterson, T. Proffen, I. K. Jeong, S. J. L. Billinge, K. S. Choi, M. G. Kanatzidis and P. G. Radaelli, *Physical Review B*, 2001, **63**, 165211.
23. M. Emam-Ismail, M. El-Hagary, E. Ramadan, A. Matar and A. El-Taher, *Radiation Effects and Defects in Solids*, 2014, **169**, 61-72.
24. V. Ryzhikov, G. Tamulaitis, N. Starzhinskiy, L. Gal'chinetskii, A. Novickovas and K. Kazlauskas, *Journal of Luminescence*, 2003, **101**, 45-53.
25. D. Kuciauskas, C. L. Perkins, M. Nardone, C. Lee, R. Mallick and G. Xiong, *Solar RRL*, 2023, **7**, 2300073.
26. M. A. Scarpulla, B. McCandless, A. B. Phillips, Y. Yan, M. J. Heben, C. Wolden, G. Xiong, W. K. Metzger, D. Mao, D. Krasikov, I. Sankin, S. Grover, A. Munshi, W. Sampath, J. R. Sites, A. Bothwell, D. Albin, M. O. Reese, A. Romeo, M. Nardone, R. Klie, J. M. Walls, T. Fiducia, A. Abbas and S. M. Hayes, *Solar Energy Materials and Solar Cells*, 2023, **255**, 112289.
27. S. G. Kumar and K. S. R. K. Rao, *Energy & Environmental Science*, 2014, **7**, 45-102.
28. B. Späth, J. Fritsche, A. Klein and W. Jaegermann, *Applied Physics Letters*, 2007, **90**.
29. C. P. Muzzillo, M. O. Reese, C. Lee and G. Xiong, *Small*, 2023, **19**, 2301939.
30. Y. Fan, *Applied Physics Letters*, 1995, **67**, 1739-1741.
31. W. Faschinger, S. Ferreira and H. Sitter, *Applied Physics Letters*, 1994, **64**, 2682-2684.
32. W. Lin, B. X. Yang, S. P. Guo, A. Elmoumni, F. Fernandez and M. C. Tamargo, *Applied Physics Letters*, 1999, **75**, 2608-2610.
33. M. Strassburg, M. Strassburg, O. Schulz, U. W. Pohl, A. Hoffmann, D. Bimberg, A. G. Kontos and Y. S. Raptis, *Journal of Crystal Growth*, 2003, **248**, 50-55.
34. A. Kamata, H. Yoshida, S. Chichibu and H. Nakanishi, *Journal of Crystal Growth*, 1997, **170**, 518-522.

View Article Online
DOI: 10.1039/D6TC00099A

35. J. Dutta, R. Pal, S. Chaudhuri and A. K. Pal, *Journal of Physics D: Applied Physics*, 1994, **27**, 1538.
36. M. M. El-Nahass, B. A. Khalifa, A. M. Abd El-Rahman and R. El-Ariny, *Applied Physics A*, 1996, **63**, 81-86.
37. M. Emam-Ismail, M. El-Hagary, E. R. Shaaban and A. M. Al-Hedeib, *Journal of Alloys and Compounds*, 2012, **532**, 16-24.
38. R. Jeyakumar, G. K. Chadda, S. T. Lakshmikumar and A. C. Rastogi, *Materials Research Bulletin*, 1999, **34**, 109-114.
39. K. R. Murali, S. Florence and R. John, *ECS Transactions*, 2012, **41**, 81.
40. A. P. Pardo González and J. Torres, *Thin Solid Films*, 2018, **660**, 421-427.
41. E. R. Shaaban, M. El-Hagary, M. Emam-Ismail, A. M. Abd Elnaeim, S. H. Moustafa and A. Adel, *Materials Science in Semiconductor Processing*, 2015, **39**, 735-741.
42. E. R. Shaban, M. Emam-Ismail, M. El-Hagary, A. M. Abd Elnaeim and A. Adel, *ANGLISTICUM. Journal of the Association-Institute for English Language and American Studies*, 2016, **3**.
43. J. Suthagar and K. J. Suthan, *Proceedings of the International Conference Nanomaterials: Applications and Properties*, 2012, 03TF08-03TF08.
44. B. K. Yadav, P. Singh, C. P. Yadav and D. K. Pandey, *Phase Transitions*, 2021, **94**, 326-337.
45. C. L. Perkins, S.-H. Lee, X. Li, S. E. Asher and T. J. Coutts, *Journal of Applied Physics*, 2005, **97**, 034907.
46. A. Nassour, *Computational Materials Science*, 2013, **77**, 403-407.
47. J. Pellicer-Porres, A. Polian, A. Segura, V. Muñoz-Sanjosé, A. Di Cicco and A. Traverse, *Journal of Applied Physics*, 2004, **96**, 1491-1498.
48. M. H. Tsai, F. C. Peiris, S. Lee and J. K. Furdyna, *Physical Review B*, 2002, **65**, 235202.
49. A. C. Aten, *Journal of Physics and Chemistry of Solids*, 1967, **28**, 1340-1342.
50. A. Ebina, M. Yamamoto and T. Takahashi, *Physical Review B*, 1972, **6**, 3786-3791.
51. S. Fujiwara and M. Fukai, *Journal of the Physical Society of Japan*, 1966, **21**, 1463-1464.
52. S. Larach, R. E. Shrader and C. F. Stocker, *Physical Review*, 1957, **108**, 587-589.
53. M. Yamamoto, A. Ebina and T. Takahashi, *Japanese Journal of Applied Physics*, 1973, **12**, 232.
54. M. J. S. P. Brasil, R. E. Nahory, F. S. Turco-Sandroff, H. L. Gilchrist and R. J. Martin, *Applied Physics Letters*, 1991, **58**, 2509-2511.
55. B. Freytag, P. Pavone, U. Rössler, K. Wolf, S. Lankes, G. Schötz, A. Naumov, S. Jilka, H. Stanzl and W. Gebhardt, *Solid State Communications*, 1995, **94**, 103-106.
56. B. E. Ponga, J. Calas, M. Averous, T. Cloitre, O. Briot, B. Gil and R. L. Aulombard, *MRS Proceedings*, 1992, **263**, 371.
57. M. C. Tamargo, M. J. S. P. Brasil, R. E. Nahory, R. J. Martin, A. L. Weaver and H. L. Gilchrist, *Semiconductor Science and Technology*, 1991, **6**, A8.

View Article Online
DOI: 10.1039/D6TC00099A

58. F. S. Turco-Sandroff, R. E. Nahory, M. J. S. P. Brasil, R. J. Martin, R. Beserman, L. A. Farrow, J. M. Worlock and A. L. Weaver, *Journal of Crystal Growth*, 1991, **111**, 762-766.
59. J. E. Bernard and A. Zunger, *Physical Review B*, 1986, **34**, 5992-5995.
60. J. E. Bernard and A. Zunger, *Physical Review B*, 1987, **36**, 3199-3228.
61. H. C. Poon, Z. C. Feng, Y. P. Feng and M. F. Li, *Journal of Physics: Condensed Matter*, 1995, **7**, 2783.
62. S. H. Wei and A. Zunger, *Journal of Applied Physics*, 1995, **78**, 3846-3856.
63. A. Zaoui, M. Certier, M. Ferhat, O. Pagès and H. Aourag, *Journal of Crystal Growth*, 1998, **184-185**, 1090-1094.
64. Y. Zhu, S. H. Zhang, X. Y. Zhang, A. M. Hao, S. L. Zhang, F. Yang, J. K. Yang and R. P. Liu, *Computational Materials Science*, 2011, **50**, 2745-2749.
65. S. Chanda, *Bulletin of Materials Science*, 2025, **48**, 92.
66. S. Chanda, D. Ghosh, B. Debnath, M. Debbarma, R. Bhattacharjee and S. Chattopadhyaya, *Journal of Computational Electronics*, 2020, **19**, 1-25.
67. D. Ghosh, S. Chanda, B. Debnath, M. Debbarma, R. Bhattacharjee and S. Chattopadhyaya, *Applied Physics A*, 2019, **125**, 644.
68. R. Malki, A. Tebboune, L. Ghalouci, A. Saim and A. H. Belbachir, *Revista Mexicana de Fisica*, 2021, **67**, 041002.
69. K. Makhratchev, K. J. Price, X. Ma, D. A. Simmons, J. Drayton, K. Ludwig, A. Gupta, R. G. Bohn and A. D. Compaan, *Conference Record of the Twenty-Eighth IEEE Photovoltaic Specialists Conference - 2000 (Cat. No.00CH37036)*, 2000, DOI: 10.1109/PVSC.2000.915874, 475-478.
70. A. E. Rakhshani and S. Thomas, *Journal of Materials Science*, 2013, **48**, 6386-6392.
71. T. M. Shimpi, J. Drayton, D. E. Swanson and W. S. Sampath, *Journal of Electronic Materials*, 2017, **46**, 5112-5120.
72. N. E. Vázquez-Barragán, R. Olvera-Rivas, L. Marasamy, J. G. Quiñones-Galván, J. Santos-Cruz, A. Guillen-Cervantes, G. Contreras-Puente and F. de Moure-Flores, *Materials Science and Engineering: B*, 2023, **296**, 116695.
73. S. Gupta, *Investigating the impact of Bulk and Surface Recombination on Open-circuit Voltage in Thin-film Cd(Se,Te) Photovoltaic devices: A Computational approach*, Bowling Green State University, 2024.
74. B. B. He, *Powder Diffraction*, 2018, **33**, 147-155.
75. D. B. Chesnokova and B. N. Ormont, *Inorganic Materials*, 1970, **6**, 1639-1640.
76. K. Shalimova, A. Andrushk, I. Spynules and B. Seredins, *Soviet Physics Crystallography*, 1965, **9**.
77. Y. S. Park and F. L. Chan, *Journal of Applied Physics*, 1965, **36**, 800-801.
78. A. A. Andreev, M. F. Bulanyj, S. A. Golikov and L. A. Mozharovskij, *Zhurnal Neorganicheskoj Khimii*, 1995, **40**, 1079-1082.
79. J. I. Pankove, *Optical processes in semiconductors*, Courier Corporation, 1972.
80. S. Tougaard, *Journal of Vacuum Science & Technology A*, 2020, **39**.
81. M. M. Beerbom, B. Lägel, A. J. Cascio, B. V. Doran and R. Schlaf, *Journal of Electron Spectroscopy and Related Phenomena*, 2006, **152**, 12-17.

View Article Online
DOI: 10.1039/D6TC00099A

82. J. Endres, D. A. Egger, M. Kulbak, R. A. Kerner, L. Zhao, S. H. Silver, G. Hodes, B. P. Rand, D. Cahen, L. Kronik and A. Kahn, *The Journal of Physical Chemistry Letters*, 2016, **7**, 2722-2729.
83. E. M. Miller, D. M. Kroupa, J. Zhang, P. Schulz, A. R. Marshall, A. Kahn, S. Lany, J. M. Luther, M. C. Beard, C. L. Perkins and J. van de Lagemaat, *ACS Nano*, 2016, **10**, 3302-3311.
84. J. F. Moulder and J. Chastain, *Handbook of X-ray Photoelectron Spectroscopy: A Reference Book of Standard Spectra for Identification and Interpretation of XPS Data*, Physical Electronics Division, Perkin-Elmer Corporation, 1992.

View Article Online
DOI: 10.1039/D6TC00099A

The data supporting this article have been included as part of the Supplementary Information.